NASA TECHNICAL NOTE

NASA TN D-6240

REAL-GAS EFFECTS ON THE DRAG AND TRAJECTORIES OF A NONLIFTING 140° CONICAL AEROSHELL DURING MARS ENTRY

by Dennis O. Allison and Percy J. Bobbitt

Langley Research Center
Hampton, Va. 23365

NATIONAL AERONAUTICS AND SPACE ADMINISTRATION • WASHINGTON, D. C. • FEBRUARY 1971

1. Report No.	2. Government Accession No.	3. Recipient's Catalog No.
NASA TN D-6240		

4. Title and Subtitle
REAL-GAS EFFECTS ON THE DRAG AND TRAJECTORIES OF A NONLIFTING 140° CONICAL AEROSHELL DURING MARS ENTRY

5. Report Date
February 1971

6. Performing Organization Code

7. Author(s)
Dennis O. Allison and Percy J. Bobbitt

8. Performing Organization Report No.
L-7522

9. Performing Organization Name and Address
NASA Langley Research Center
Hampton, Va. 23365

10. Work Unit No.
129-01-22-10

11. Contract or Grant No.

12. Sponsoring Agency Name and Address
National Aeronautics and Space Administration
Washington, D.C. 20546

13. Type of Report and Period Covered
Technical Note

14. Sponsoring Agency Code

15. Supplementary Notes

16. Abstract

The present paper is a study of the influence of real-gas effects on the drag and trajectories of a 140° conical aeroshell during entry into five model Mars atmospheres. Drag coefficients are obtained by using an approximate technique which enables their determination at every point along a trajectory with reasonable computer time. The standard point mass trajectory equations are used and a spectrum of entry conditions are considered that consist of velocities of 4.27, 4.57 and 4.88 km/sec (14 000, 15 000, and 16 000 ft/sec) and entry flight-path angles of 13.5°, 15°, and 17.5°. All calculations were made for an entry spacecraft with a ratio of mass to maximum cross-sectional area of 76.5 kg/m^2 (0.487 slug/ft^2). It is shown that a single curve may be chosen to represent the drag coefficient variations within 2 percent accuracy for all five model atmospheres and all the entry conditions considered.

17. Key Words (Suggested by Author(s))	18. Distribution Statement
Real-gas effects Mass entry trajectory Conical aeroshell Blunt body drag	Unclassified – Unlimited

19. Security Classif. (of this report)	20. Security Classif. (of this page)	21. No. of Pages	22. Price*
Unclassified	Unclassified	28	$3.00

*For sale by the National Technical Information Service, Springfield, Virginia 22151

REAL-GAS EFFECTS ON THE DRAG AND TRAJECTORIES OF A NONLIFTING 140° CONICAL AEROSHELL DURING MARS ENTRY

By Dennis O. Allison and Percy J. Bobbitt
Langley Research Center

SUMMARY

The present paper is a study of the influence of real-gas effects on the drag and trajectories of a 140° conical aeroshell during entry into five model Mars atmospheres. Drag coefficients are obtained by using an approximate technique which enables their determination at every point along a trajectory with reasonable computer time. The standard point mass trajectory equations are used and a spectrum of entry conditions are considered that consist of velocities of 4.27, 4.57, and 4.88 km/sec (14 000, 15 000, and 16 000 ft/sec) and entry flight-path angles of 13.5°, 15°, and 17.5°. All calculations were made for an entry spacecraft with a ratio of mass to maximum cross-sectional area of 76.5 kg/m^2 (0.487 slug/ft^2). It is shown that a single curve may be chosen to represent the drag coefficient variations within 2 percent accuracy for all five model atmospheres and all the entry conditions considered.

INTRODUCTION

Most of the mission analysis research on the atmospheric-entry phase of a Mars lander mission has been done with a constant ballistic parameter. (For example, see refs. 1 and 2.) Since no mass losses or area changes are assumed in these analyses, a constant ballistic parameter implies a constant drag coefficient. Ordinarily, this constant drag coefficient is taken to be the hypersonic value measured in wind tunnels with air as a test medium. In reality, however, the drag coefficient of a body changes during entry and the manner in which it changes depends on the vehicle speed and the atmospheric composition, pressure, and temperature. These drag changes result from the excitation of the higher degrees of freedom of the gas, such as vibration and dissociation (commonly called real-gas effects), in the shock layer ahead of the body where the gas is much denser and hotter than in the ambient stream. For a predominantly CO_2 gas mixture such as the Mars atmosphere, real-gas effects on the drag are larger than those encountered in air for the same velocity and ambient conditions; they can have a significant effect on an entry vehicle's trajectory.

The purpose of the present paper is to assess the magnitude of the real-gas effects on the drag coefficient for a 140° conical aeroshell during entry into five model Mars atmospheres.* The model Mars atmospheres are designated and defined as follows:

Max H_ρ atmosphere	atmosphere with maximum average density scale height
Max ρ_s atmosphere	atmosphere with maximum density near surface
Mean atmosphere	mean model atmosphere
Min H_ρ atmosphere	atmosphere with minimum average density scale height
Min ρ_s atmosphere	atmosphere with minimum density near surface

Drag coefficients are obtained by using an approximate technique which enables their determination at every point along a trajectory with reasonable computer time. The standard point mass trajectory equations (see appendix A) are used and a spectrum of orbital entry conditions are considered at an altitude of 244 km (800 000 ft) including velocities of 4.27 to 4.88 km/sec (14 000 to 16 000 ft/sec) and entry flight-path angles of 13.5° to 17.5°. The entry spacecraft is assumed to have a ratio of mass to maximum cross-sectional area of 76.5 kg/m^2 (0.487 slug/ft^2) in all calculations.

SYMBOLS

Trajectory parameters were originally chosen in the U.S. Customary Units and the model atmospheres selected were in the SI Units. However, these quantities are expressed in both systems of units for the convenience of the reader.

A	maximum cross-sectional area of the aeroshell, m^2 (ft^2)
C_D	drag coefficient, $\dfrac{\text{Drag force}}{\frac{1}{2}\rho_\infty V_\infty{}^2 A}$
g	acceleration of gravity, m/sec^2 (ft/sec^2)
g_s	acceleration of gravity near the surface of Mars, m/sec^2 (ft/sec^2)

*Mars model atmospheres developed by George P. Wood of Langley Research Center.

h_∞	free-stream static enthalpy per unit mass, m^2/sec^2 (ft^2/sec^2)
h_S	static enthalpy per unit mass behind the shock, m^2/sec^2 (ft^2/sec^2)
H	altitude, km (ft)
M	mass of entry spacecraft, kg (slugs)
M_∞	free-stream Mach number
M_U	molecular mass of undissociated gas mixture
N_{CO_2}	number of moles of carbon dioxide per unit mass in undissociated gas mixture
N_{Re}	Reynolds number based on base diameter of model
p_∞	free-stream pressure, N/m^2 (lb/ft^2)
p_o	reference pressure, 0.1013 MN/m^2 (2116 lb/ft^2)
p_S	pressure behind shock, N/m^2 (lb/ft^2)
q_∞	free-stream dynamic pressure, $\frac{1}{2}\rho_\infty V_\infty^2$, N/m^2 (lb/ft^2)
r_s	mean radius of Mars, km (ft)
R_o	universal gas constant, 8315 kg-m^2/sec^2-^oK-(kg-mole) (49 720 lb-ft^2/sec^2-^oR-(lb-mole))
R_U	gas constant for undissociated gas mixture, R_o/M_U, m^2/sec^2-^oK (ft^2/sec^2-^oR)
t	time, sec
T_∞	free-stream temperature, ^oK (^oR)
T_o	reference temperature, 273.2° K (491.7° R)

T_S temperature behind shock, ^{o}K (^{o}R)

u_∞ free-stream velocity component normal to shock wave, m/sec (ft/sec)

u_S normal component of velocity behind shock, m/sec (ft/sec)

V_∞ free-stream velocity, m/sec (ft/sec)

V_E entry velocity, m/sec (ft/sec)

γ ratio of specific heats

γ_e effective value of γ, defined by equation (1)

Δt time increment, sec

θ shock inclination angle, deg

ρ_∞ free-stream density, kg/m^3 ($slugs/ft^3$)

ρ_o reference density, $M_U p_o / R_o T_o$, kg/m^3 ($slugs/ft^3$)

ρ_S density behind shock, kg/m^3 ($slugs/ft^3$)

ϕ flight-path angle, deg

ϕ_E entry flight-path angle, deg

DRAG COEFFICIENT DETERMINATION

A value of the drag coefficient C_D is required in the equations of motion (appendix A) in order to determine the position and velocity of an entry body after an increment of time Δt. Figure 1 presents experimental drag coefficient data (refs. 3 and 4) for Mach numbers from 2 to 10 for a 140^{o} conical aeroshell obtained in two air facilities ($\gamma = 1.4$). It shows that the drag coefficient is essentially constant and implies that there are no significant real-gas effects in air up to a Mach number of 10. However, in a Mars-like atmosphere composed largely of carbon dioxide, real-gas effects are expected to be important even in this speed range. In the remainder of this section, a procedure is outlined whereby approximate real-gas corrections to air-drag data may be applied for various atmospheric compositions.

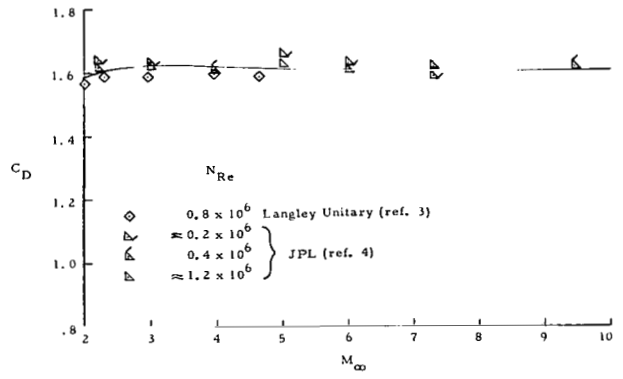

Figure 1.- Experimental variation of drag coefficient with Mach number for a 140^o conical aeroshell in air.

There are three basic steps in the present approach for obtaining a real-gas drag coefficient for the model Mars atmosphere being "entered." The first step uses the instantaneous velocity, free-stream conditions, and equilibrium thermodynamic properties behind the shock in solving the oblique-shock equations to obtain the real-gas shock density ratio. (See appendix B.) The second step uses this shock density ratio, a prescribed shock inclination angle (taken to be 70^o), and free-stream Mach number to determine an effective value of the ratio of specific heats γ_e from the perfect-gas relation

$$\gamma_e = \frac{(M_\infty \sin \theta)^2\left(\frac{\rho_S}{\rho_\infty} + 1\right) - 2\frac{\rho_S}{\rho_\infty}}{(M_\infty \sin \theta)^2\left(\frac{\rho_S}{\rho_\infty} - 1\right)} \tag{1}$$

(Note that eq. (1) is the solution obtained from the equation given in ref. 5 for the perfect-gas density jump across an oblique shock.) In the third step, the value of γ_e is used to determine the drag coefficient from a curve provided in figure 2.

The variation of C_D with γ_e in figure 2 is based on a theoretical perfect-gas drag curve obtained by using the method of reference 6 for a 140^o conical aeroshell. The theoretical results were corrected to agree with the wind-tunnel data in figure 1 in which $\gamma = 1.4$ and $C_D = 1.61$. The corrected C_D curve is in reasonable agreement with the carbon tetrafluoride (CF_4) data in reference 7 where for a γ of about 1.16 to 1.17, C_D is in the range of 1.7 to 1.76. Since the flow behind the shock becomes supersonic when γ_e decreases to a value of approximately 1.12, theoretical C_D values could not be obtained from the method of reference 6 below this value. Consequently, an arbitrary fairing from the C_D value at $\gamma_e = 1.12$ to the Newtonian value of $C_D = 1.766$ at $\gamma_e = 1$ was employed. The use of perfect-gas results with γ_e from real-gas shock

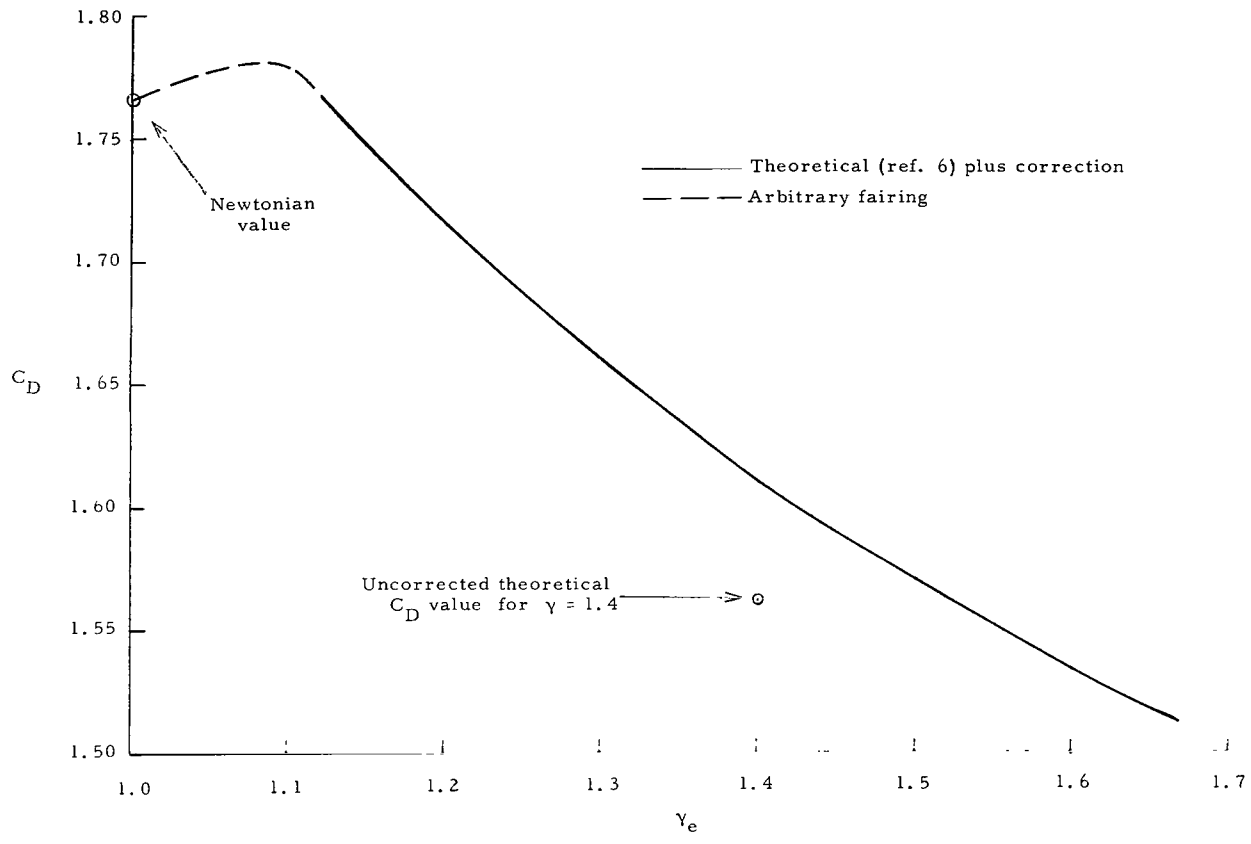

Figure 2.- Theoretical variation (plus empirical correction) of drag coefficient with effective ratio of specific heats for a 140° conical aeroshell.

calculations is permissible since the ratio of specific heats is nearly constant in the shock layer ahead of extremely blunt bodies such as the 140° cone.

REAL-GAS THERMODYNAMIC PROPERTIES

The free-stream real-gas effects are molecular rotation and vibration whereas for the higher temperature gas behind the shock molecular rotation, vibration, electronic excitation, dissociation, and ionization were considered. All equations and thermochemical constants for computing thermodynamic properties from temperature, pressure, and elemental composition (relative amounts of C, O, and Ar of which the gas mixture is composed) are given in references 8 and 9. Surface conditions for the five model Mars atmospheres treated in the present paper (Max H_ρ, Max ρ_S, Mean, Min H_ρ, and Min ρ_S atmospheres) are given in table I.

TABLE I.- ATMOSPHERIC CONDITIONS NEAR THE MEAN SURFACE FOR THE FIVE MODEL MARS ATMOSPHERES

Parameter	Conditions for –				
	Min ρ_S atmosphere	Min H_ρ atmosphere	Mean atmosphere	Max ρ_S atmosphere	Max H_ρ atmosphere
Density scale height,					
km	18.3	11.9	15.8	10.8	19.6
ft	60 000	39 000	51 800	35 400	64 300
Density,					
kg/m^3	0.00756	0.0118	0.0136	0.0286	0.0184
g/cm^3	7.56×10^{-6}	1.18×10^{-5}	1.36×10^{-5}	2.86×10^{-5}	1.84×10^{-5}
$slug/ft^3$	1.47×10^{-5}	2.29×10^{-5}	2.64×10^{-5}	5.55×10^{-5}	3.57×10^{-5}
Pressure,					
N/m^2	400	400	600	1000	1000
mb	4	4	6	10	10
lb/ft^2	8.35	8.35	12.5	20.9	20.9
Temperature, °K	280	180	230	180	280
Composition by mass, percent					
CO_2	100	100	88	73	73
Ar	0	0	12	27	27
Composition by volume, percent					
CO_2	100	100	87	71	71
Ar	0	0	13	29	29
Molecular mass	44	44	43.5	42.8	42.8
Acceleration of gravity,					
m/sec^2	3.72	3.72	3.72	3.72	3.72
ft/sec^2	12.2	12.2	12.2	12.2	12.2
Equatorial radius,					
km	3393	3393	3393	3393	3393
ft	1.113×10^7	1.113×10^7	1.113×10^7	1.113×10^7	1.113×10^7

Free-Stream Thermodynamic Properties

Free-stream temperature, pressure, and density are plotted against altitude in figures 3 to 5 for the five models; static enthalpy and speed of sound were computed directly from free-stream composition (tables I and II) and temperature (fig. 3). The free-stream composition of each of the models is constant for altitudes up to 90 km (295 000 ft) and changes continuously at higher altitudes. Fortunately above 90 km, the density of four of the model atmospheres is so low that the variations in composition have negligible effects on the trajectories. The exception is the maximum density scale height model atmosphere (Max H_ρ atmosphere). Table II gives the altitude variation of composition for the Max H_ρ atmosphere, as table I gives only the low-altitude composition.

Thermodynamic Properties Behind the Shock

Polynomial approximations of the variations of equilibrium T_S and $h_S/R_U T_S$ with pressure and density were used behind the shock wave. A given curve fit (polynomial approximation) is only valid for a constant elemental composition (constant proportions of the elements C, O, and Ar). As noted in the last section, the composition of each model atmosphere is constant for altitudes up to 90 km (295 000 ft), and only the Max H_ρ atmosphere is important at higher altitudes.

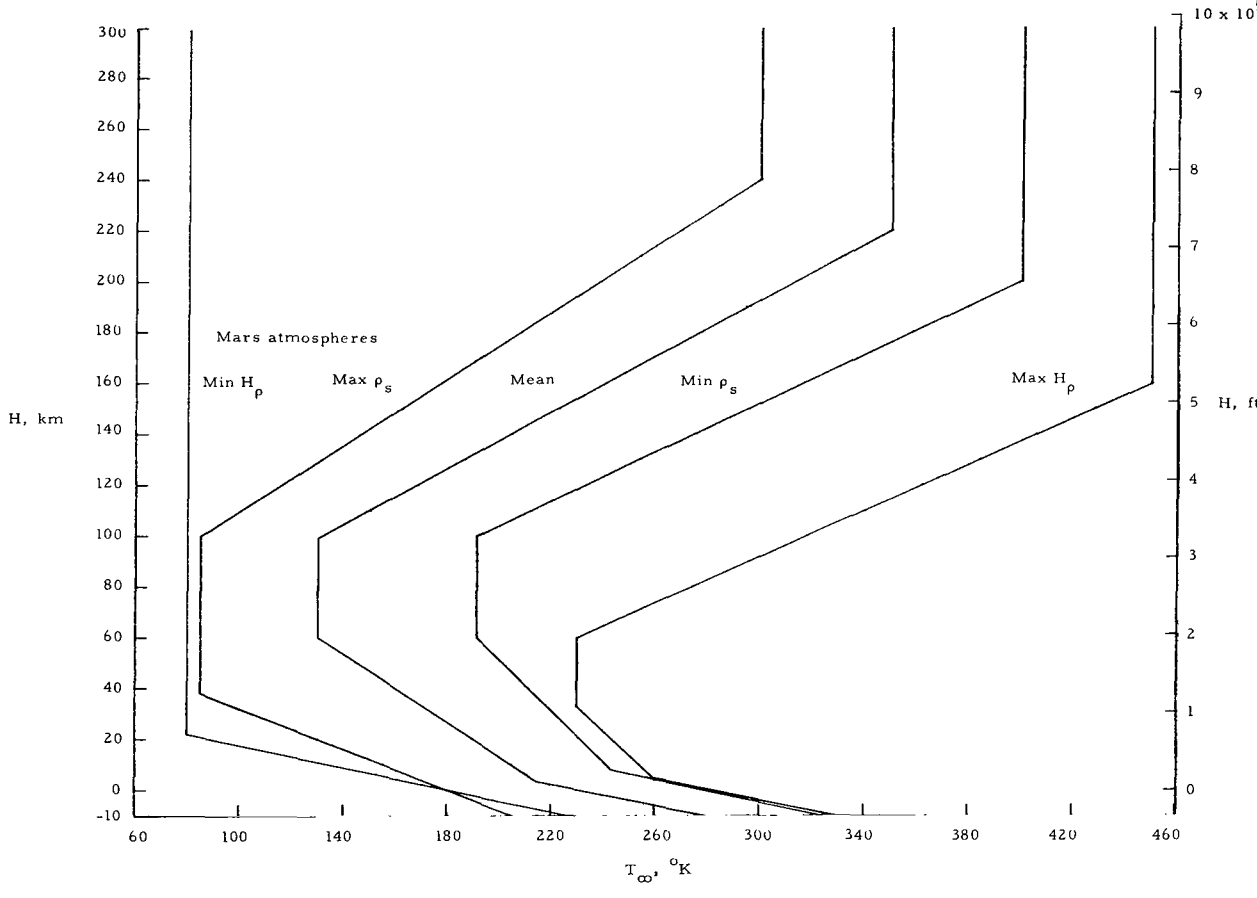

Figure 3.- Temperature profiles for the five model Mars atmospheres.

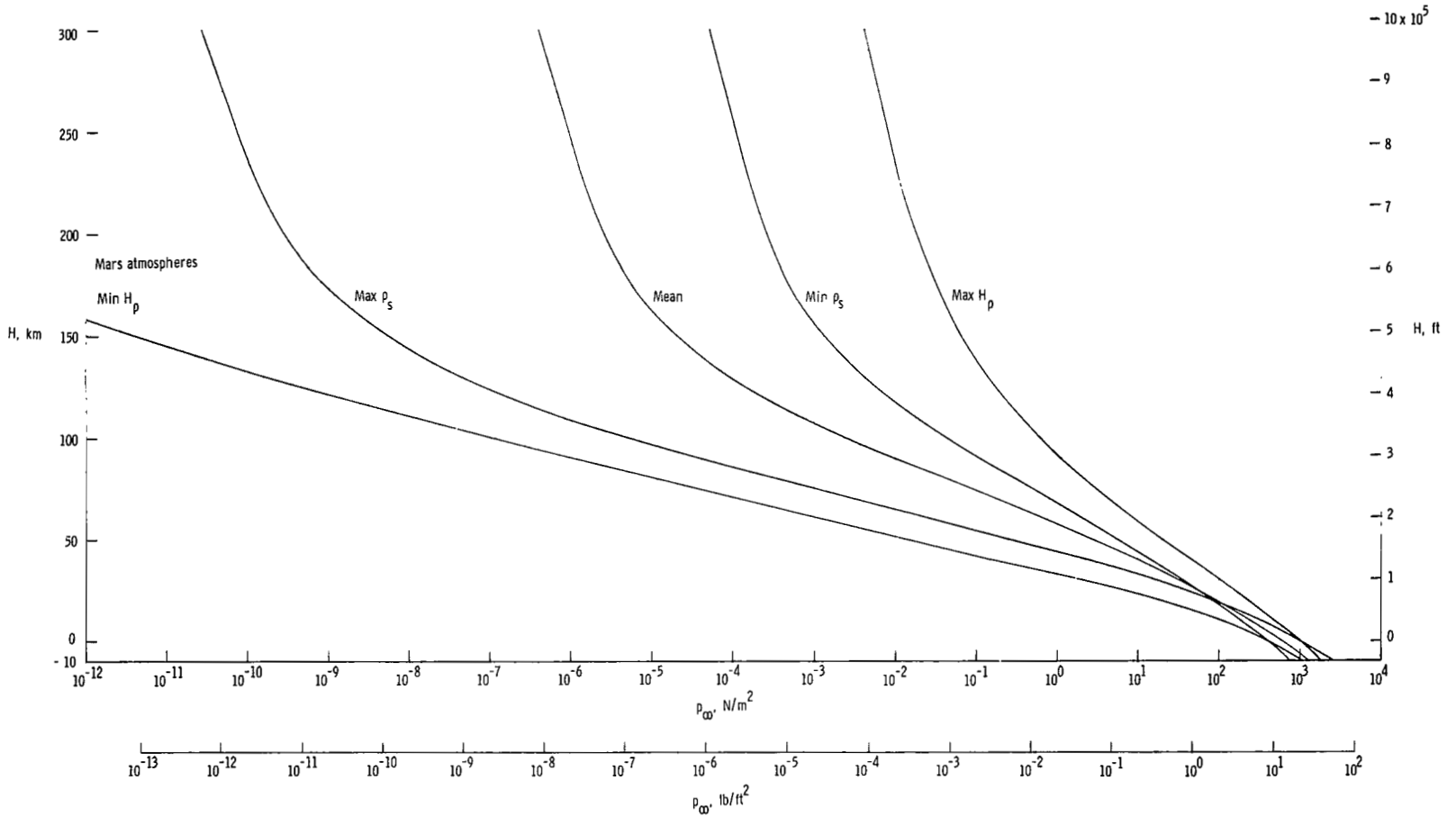

Figure 4.- Pressure profiles for the five model Mars atmospheres.

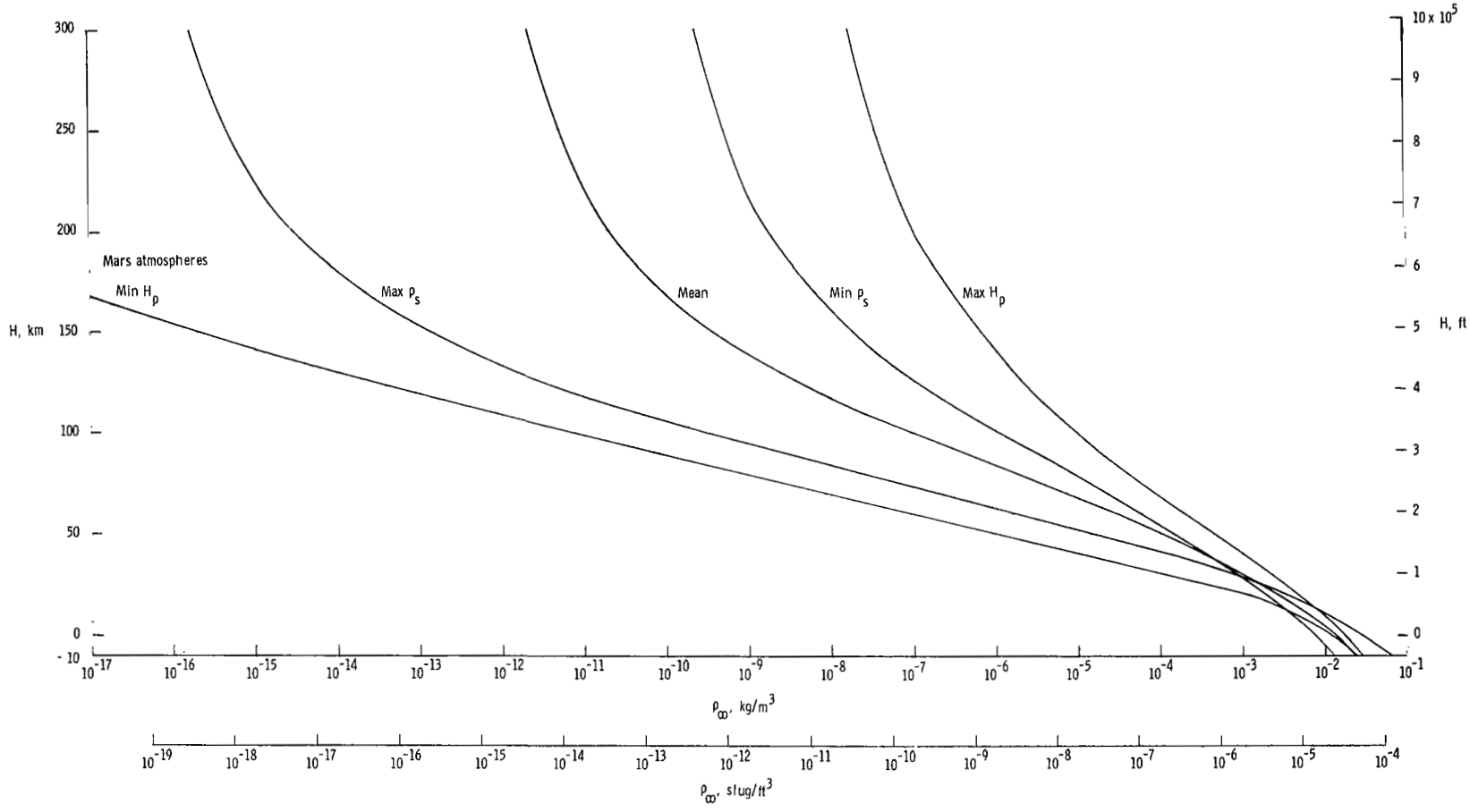

Figure 5.- Density profiles for the five model Mars atmospheres.

TABLE II.- COMPOSITION BY VOLUME OF MAX H_ρ

MODEL ATMOSPHERE

H		Composition by volume, percent			
km	ft	CO_2	CO	O	Ar
0 to 90	0 to 295 000	71.05	0	0	28.95
100	328 000	69.66	1.50	1.50	27.34
110	361 000	67.33	2.76	4.34	25.57
120	394 000	64.97	4.12	7.85	23.06
130	427 000	62.72	5.42	12.33	19.53
140	459 000	60.71	6.73	18.09	14.47
150	492 000	56.84	7.75	25.15	10.26
160	525 000	50.30	8.45	33.10	8.15
170	558 000	41.69	8.95	42.69	6.67
180	591 000	30.85	9.37	53.93	5.85
190	623 000	17.50	9.20	68.50	4.80
200	656 000	9.66	8.77	77.49	4.08
210	689 000	5.96	7.85	82.71	3.48
220	722 000	4.05	6.73	86.45	2.77
230	755 000	2.58	5.36	89.98	2.08
240	787 000	1.49	3.78	93.14	1.59
250	820 000	.30	2.01	96.69	1.00
260	853 000	0	0	99.49	.51
270	886 000	0	0	100.00	0
300	984 000	0	0	100.00	0

The Max H_ρ atmosphere required that equilibrium thermodynamic properties for three elemental compositions be used: one for the composition at altitudes up to 90 km (295 000 ft), another for the composition at 150 km (492 000 ft), and a third for that at 240 km (787 000 ft). Since the elemental composition changes continuously above 90 km (295 000 ft), linear interpolation between the thermodynamic properties of these three altitudes was utilized to obtain the properties for the other altitudes. (See appendix C for details.) The interpolation parameter for $h_S/R_U T_S$ was the molecular mass of the undissociated gas mixture, whereas that for T_S was the number of elemental moles of carbon per unit mass of the atmosphere. Errors in $h_S/R_U T_S$ and T_S due to the interpolation routine were usually less than 2 percent.

RESULTS AND DISCUSSION

Real-gas results are given for five model Mars atmospheres and a spectrum of entry conditions including orbital entry velocities of 4.27, 4.57, and 4.88 km/sec (14 000, 15 000, and 16 000 ft/sec) and entry flight-path angles of 13.5°, 15°, and 17.5°. Entry conditions are defined at an arbitrary altitude of 244 km (800 000 ft). All calculations are for a 140° conical aeroshell with $M/A = 76.5$ kg/m^2 (0.487 slug/ft^2). Figures 6 to 14 give calculated drag coefficients, dynamic pressures, and effective specific heat ratios as well as Mach numbers and flight-path angles.

Drag Variation With Altitude

The behavior of the real-gas drag coefficient as altitude changes is illustrated by figure 6(a) for the entry conditions $V_E = 4.57$ km/sec (15 000 ft/sec) and $\phi_E = 15^\circ$. For each model atmosphere, figure 6(b) locates the dynamic-pressure pulse or the altitude range where the value of the drag coefficient is most important. It is seen that at maximum dynamic pressure, the drag coefficients are in the neighborhood of $C_D = 1.75$ which is about 9 percent higher than $C_D = 1.61$ in the wind-tunnel data of figure 1.

The real-gas drag coefficient is, of course, determined from the variation of C_D with γ_e shown in figure 2. Therefore, one could construct an altitude variation of γ_e from figures 6(a) and 2. For convenience, curves for the variation of γ_e with altitude are given in figure 7 and can be used together with figure 6(b) to show that γ_e is approximately 1.14 at maximum dynamic pressure.

Drag Variation With Mach Number

Figures 8 to 12 display the variation of drag coefficient with Mach number for all five model atmospheres and all entry conditions considered. The drag coefficient curves for the Max ρ_s, Mean, Min ρ_s, and Min H_ρ atmospheres all start with a value of

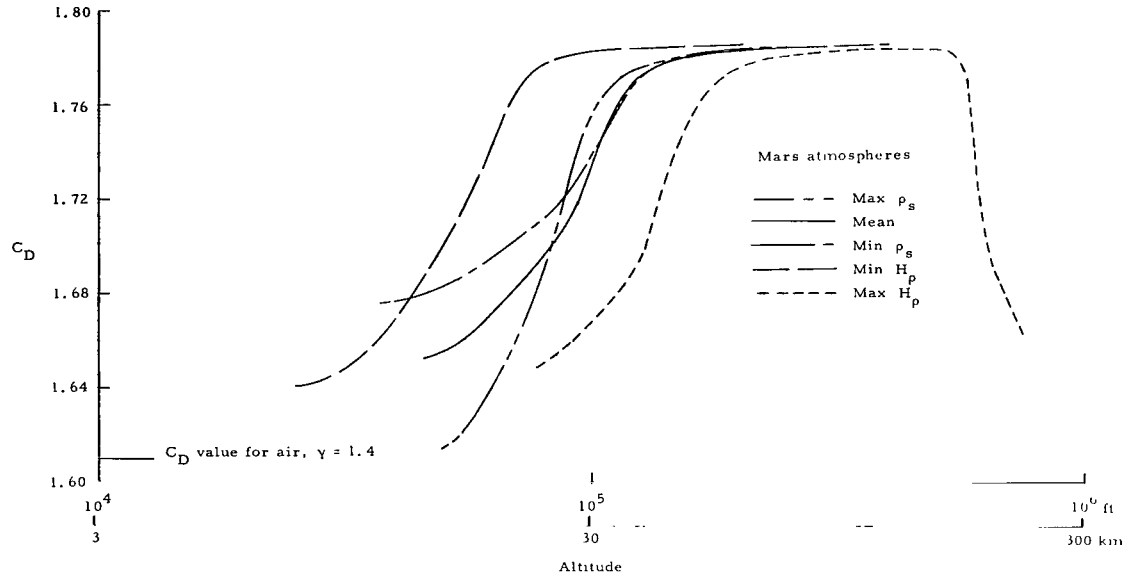

(a) Drag coefficient.

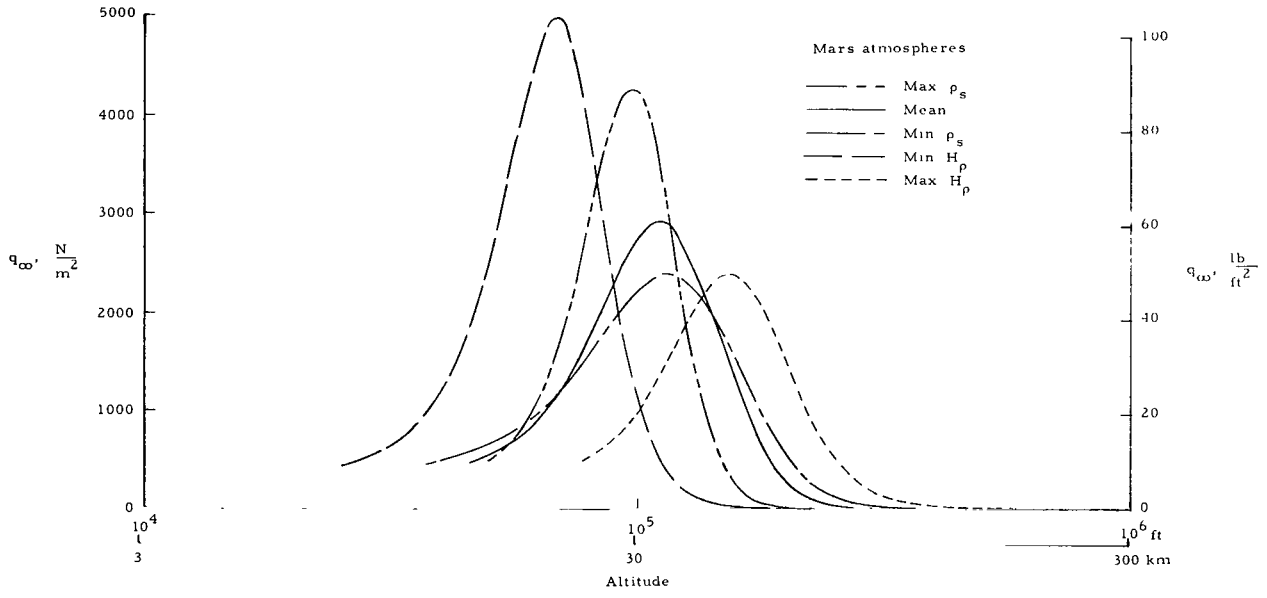

(b) Dynamic pressure.

Figure 6.- Variation with altitude of calculated drag coefficient and dynamic pressure for $\phi_E = 15^\circ$ and $V_E = 4.57$ km/sec (15 000 ft/sec) for the five model atmospheres.

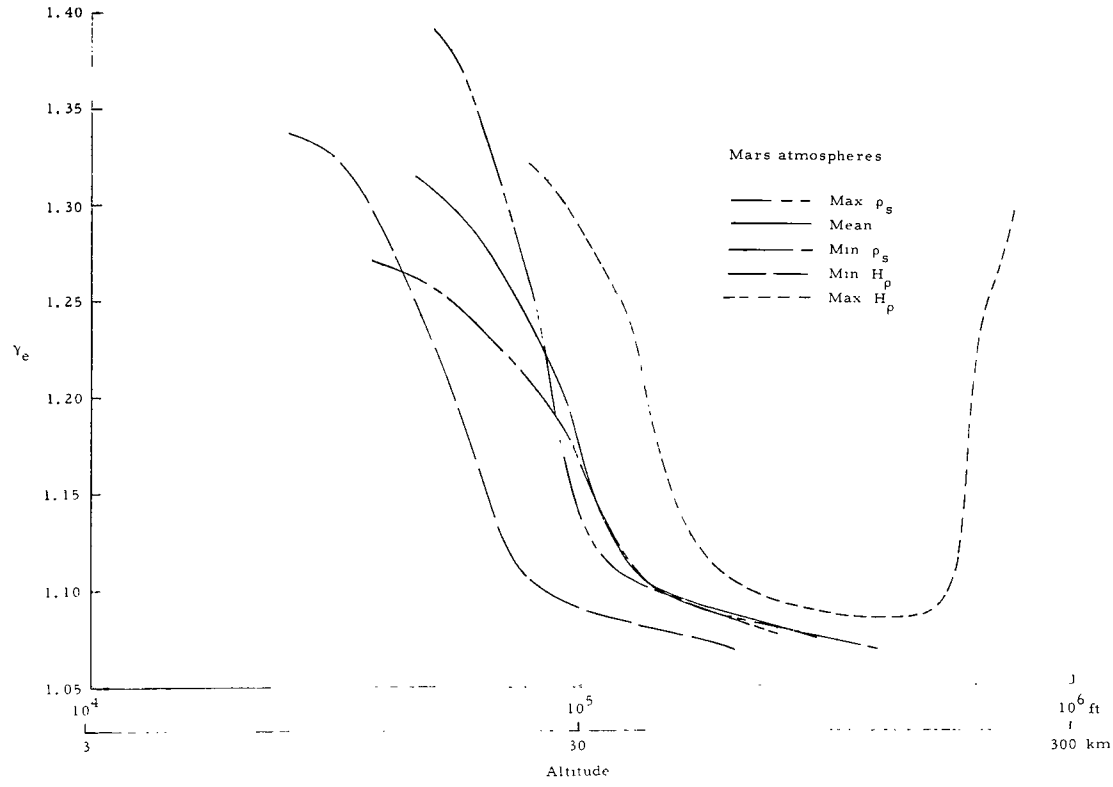

Figure 7.- Variation with altitude of effective ratio of specific heats for $\phi_E = 15^\circ$ and $V_E = 4.57$ km/sec (15 000 ft/sec) for the five model atmospheres.

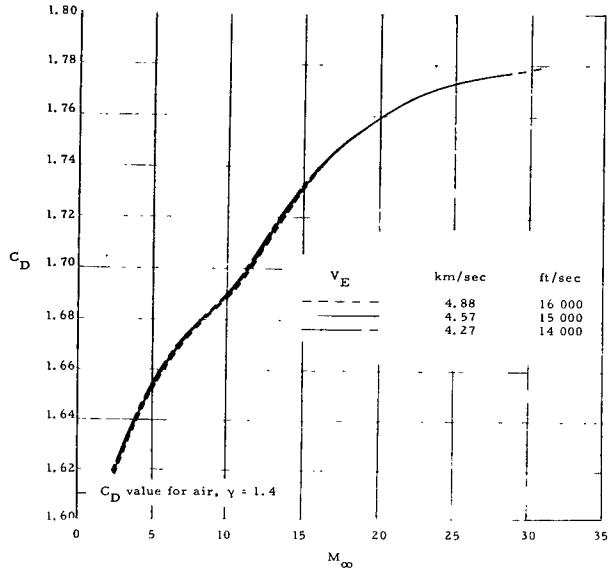

(a) Entry velocity effect for $\phi_E = 15^\circ$.

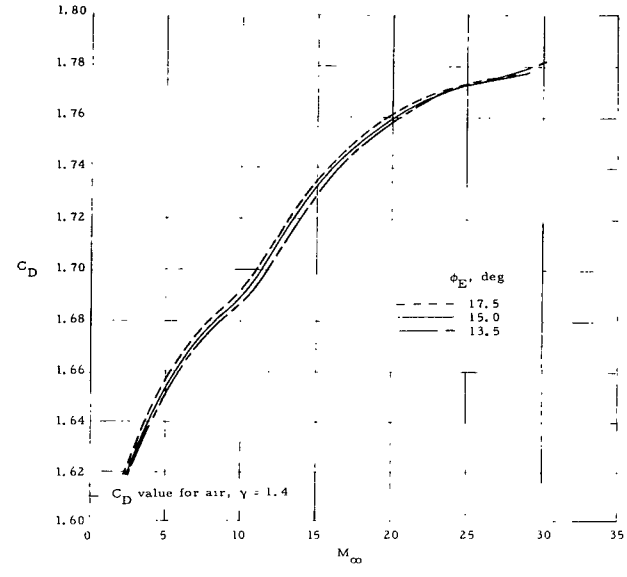

(b) Entry flight-path angle effect for $V_E = 4.57$ km/sec (15 000 ft/sec).

Figure 8.- Variation of calculated drag coefficient with Mach number for the Max ρ_s model atmosphere for three entry velocities and three entry flight-path angles.

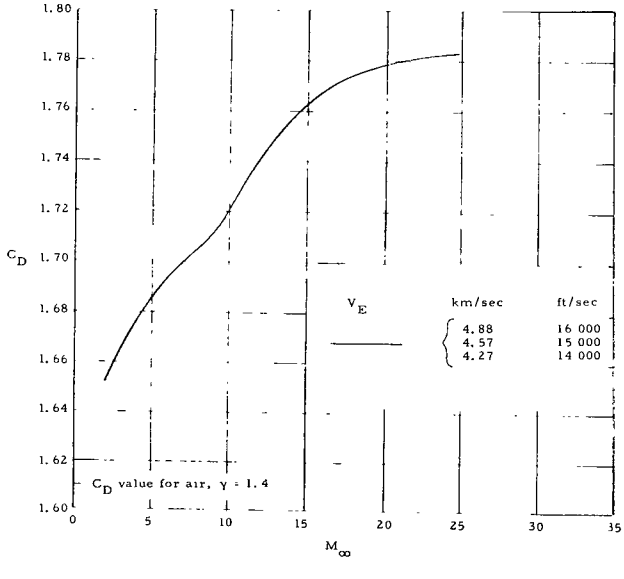

(a) Entry velocity effect for $\phi_E = 15^\circ$.

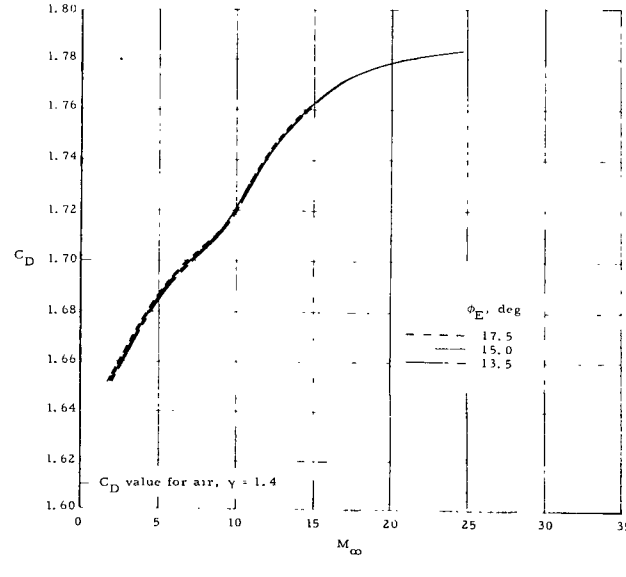

(b) Entry flight-path angle effect for $V_E = 4.57$ km/sec (15 000 ft/sec).

Figure 9.- Variation of calculated drag coefficient with Mach number for the Mean model atmosphere for three entry velocities and three entry flight-path angles.

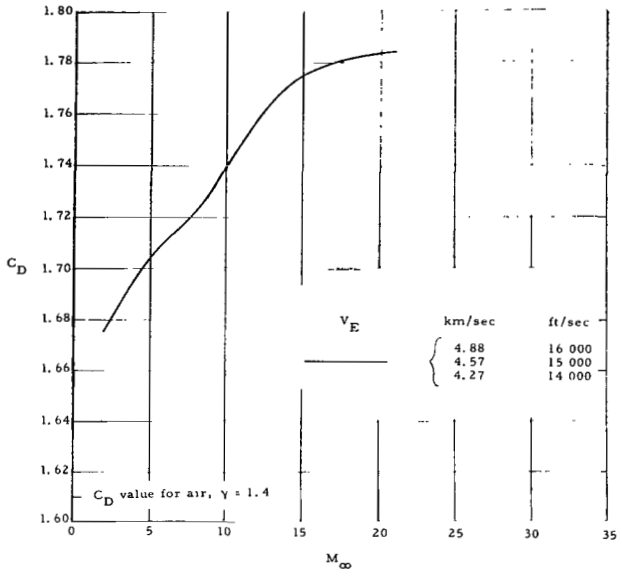

(a) Entry velocity effect for $\phi_E = 15^\circ$.

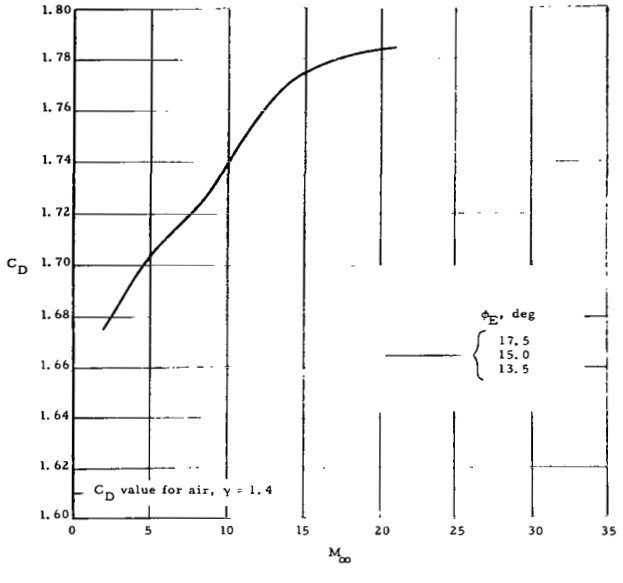

(b) Entry flight-path angle effect for $V_E = 4.57$ km/sec (15 000 ft/sec).

Figure 10.- Variation of calculated drag coefficient with Mach number for the Min ρ_S model atmosphere for three entry velocities and three entry flight-path angles.

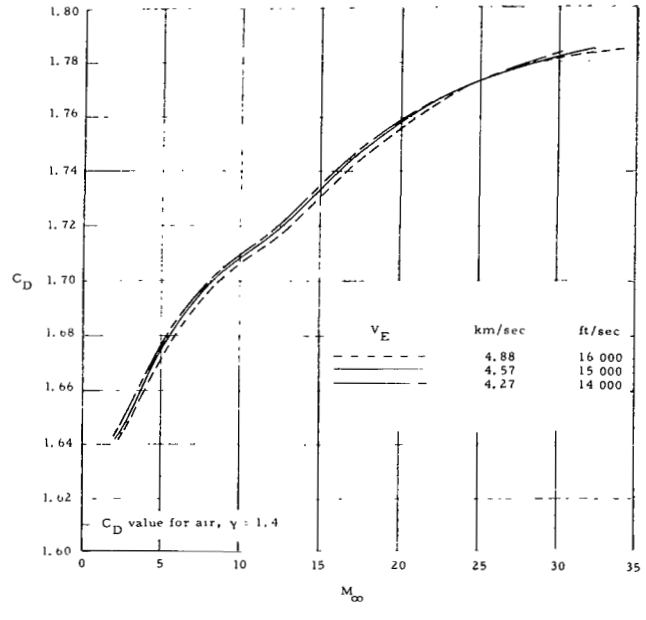

(a) Entry velocity effect for $\phi_E = 15^\circ$.

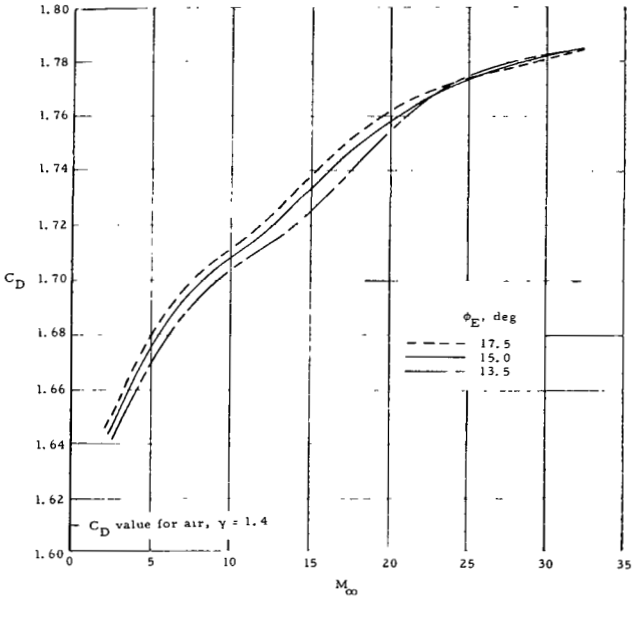

(b) Entry flight-path angle effect for $V_E = 4.57$ km/sec (15 000 ft/sec).

Figure 11.- Variation of calculated drag coefficient with Mach number for the Min H_ρ model atmosphere for three entry velocities and three entry flight-path angles.

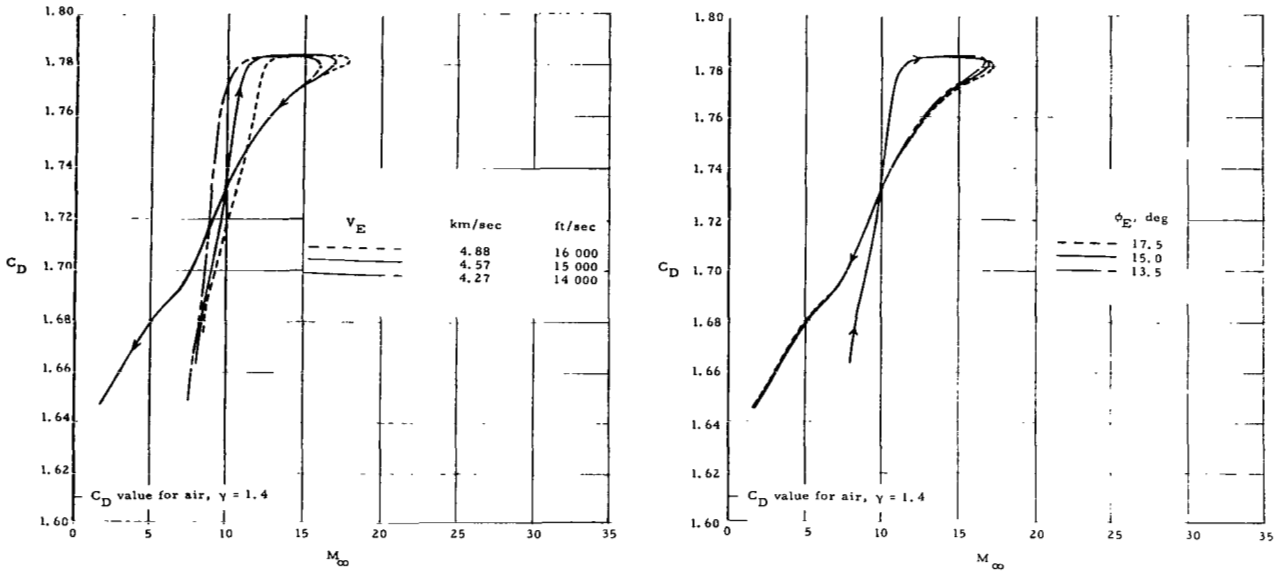

(a) Entry velocity effect for $\phi_E = 15^\circ$.

(b) Entry flight-path angle effect for $V_E = 4.57$ km/sec (15 000 ft/sec).

Figure 12.- Variation of calculated drag coefficient with Mach number for the Max H_ρ model atmosphere for three entry velocities and three entry flight-path angles.

approximately 1.78 at high Mach numbers and decrease monotonically to values varying from 1.62 to 1.67. Curves for the Max H_ρ atmosphere (fig. 12) are considerably different in character from the others because drag coefficients for this model must be computed to much higher altitudes where the temperature and, hence, the speed of sound is high and the Mach numbers are low. Furthermore, the free-stream gas at high altitude is composed of atomic oxygen so that no dissociation takes place in the shock layer ahead of the body. Density jumps across the shock are therefore lower and this condition, in turn, leads to lower drag coefficients. The high-altitude ends of the Max H_ρ curves start at a C_D of approximately 1.66 and a Mach number of about 8. As the altitude decreases, the drag coefficients and Mach numbers increase to a maximum and then decrease in a manner similar to the curves for the other atmospheres.

It is evident from figures 8 to 12 that changes in entry velocity and flight-path angle over the ranges considered result in only small or negligible differences in the variations of drag coefficient with Mach number. The largest effect of entry velocity changes occurs in the drag coefficient curves for the Max H_ρ atmosphere whereas small increments in the flight-path angle at entry have the most effect in the Min H_ρ atmosphere.

Drag coefficients for all five model atmospheres are compared in figure 13 for the entry conditions $V_E = 4.57$ km/sec (15 000 ft/sec) and $\phi_E = 15^\circ$. Ideally, one would

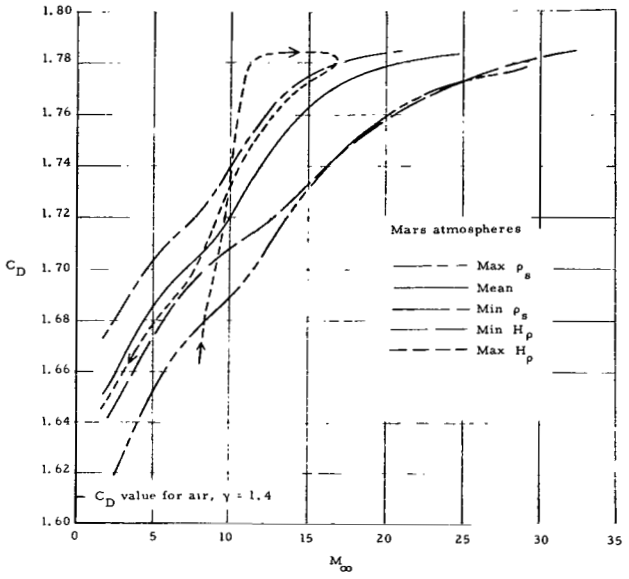

Figure 13.- Variation of calculated drag coefficient with Mach number for an entry flight-path angle of 15° and an entry velocity of 4.57 km/sec (15 000 ft/sec) for all five model atmospheres.

hope to find a single Mach number variation of drag coefficient that would be satisfactory for all Mars orbital entry trajectory calculations. If such a curve did exist, it would afford a substantial convenience in parametric studies. The magnitude of error that one would incur by using an average drag curve can be obtained from figure 13 which shows that drag coefficients increase approximately 3 percent in going from the Max ρ_s to the Min ρ_s atmospheres. An average real-gas drag curve will result then in roughly a 1.5-percent error. In the light of the uncertainties in the Mars atmosphere itself, the selection of a single drag coefficient curve, be it an average or a conservative one, for mission analysis work may be desirable.

Trajectory Comparisons

To illustrate the difference between real-gas drag coefficient trajectories and those obtained by using a constant drag coefficient of $C_D = 1.61$, figure 14 and table III have been prepared. Figure 14 shows the variations of Mach number and flight-path angle with altitude for the five model atmospheres. Inasmuch as some assumptions inherent in the present analysis become less valid with decreasing Mach number, the computations were terminated at a Mach number of 2.

Since one would expect any significant differences in the trajectory parameters to appear most pronounced after integrating over the entire trajectory (down to Mach 2 in the present calculations), pertinent numerical results are given in table III. It is seen

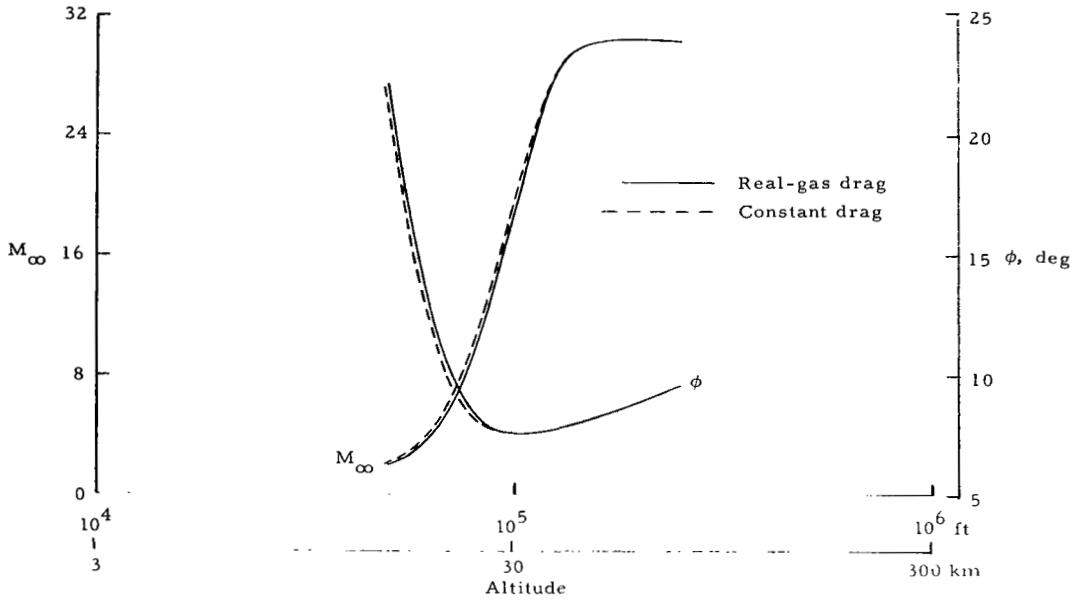

(a) Max ρ_s model atmosphere.

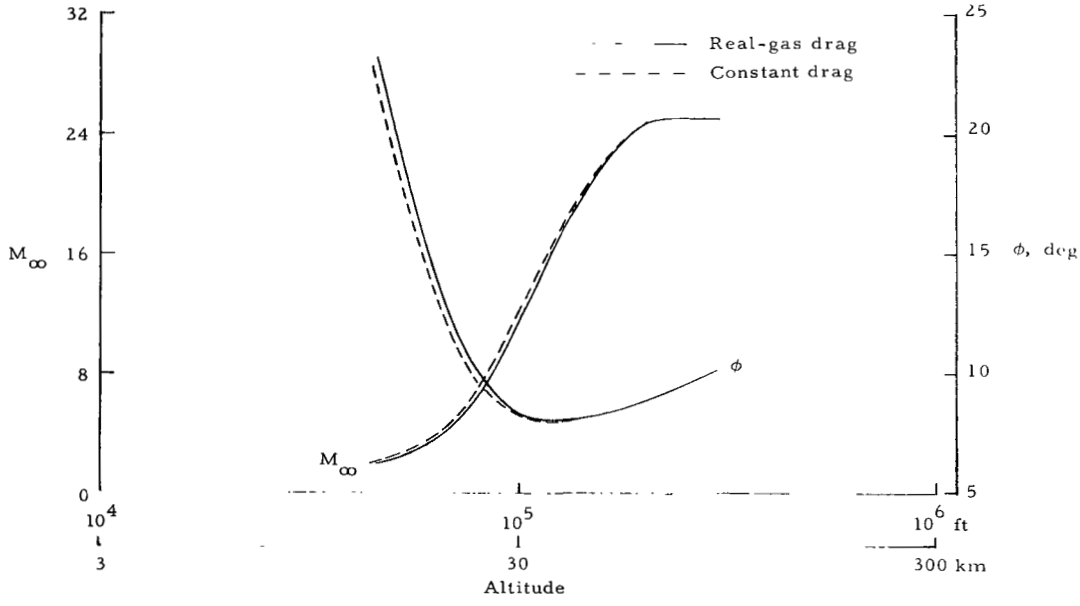

(b) Mean model atmosphere.

Figure 14.- Altitude variation of Mach number and flight-path angle for entry conditions of V_E = 4.57 km/sec (15 000 ft/sec) and $\phi_E = 15^\circ$ for the five model atmospheres. (See table III for a tabulation of trajectory parameters at a Mach number of 2.)

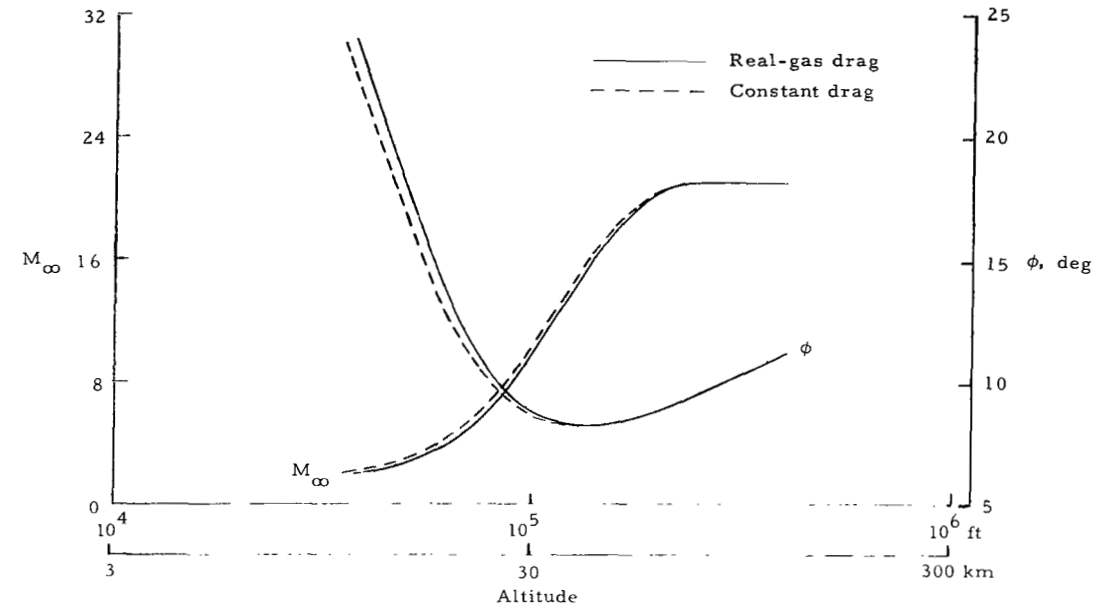

(c) Min ρ_s model atmosphere.

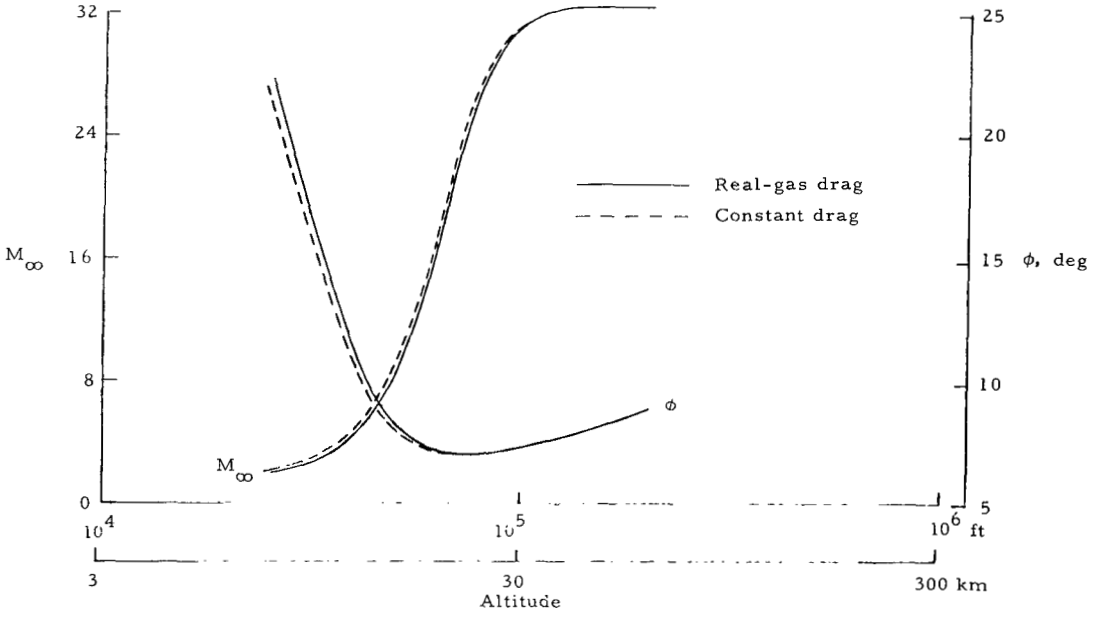

(d) Min H_ρ model atmosphere.

Figure 14.- Continued.

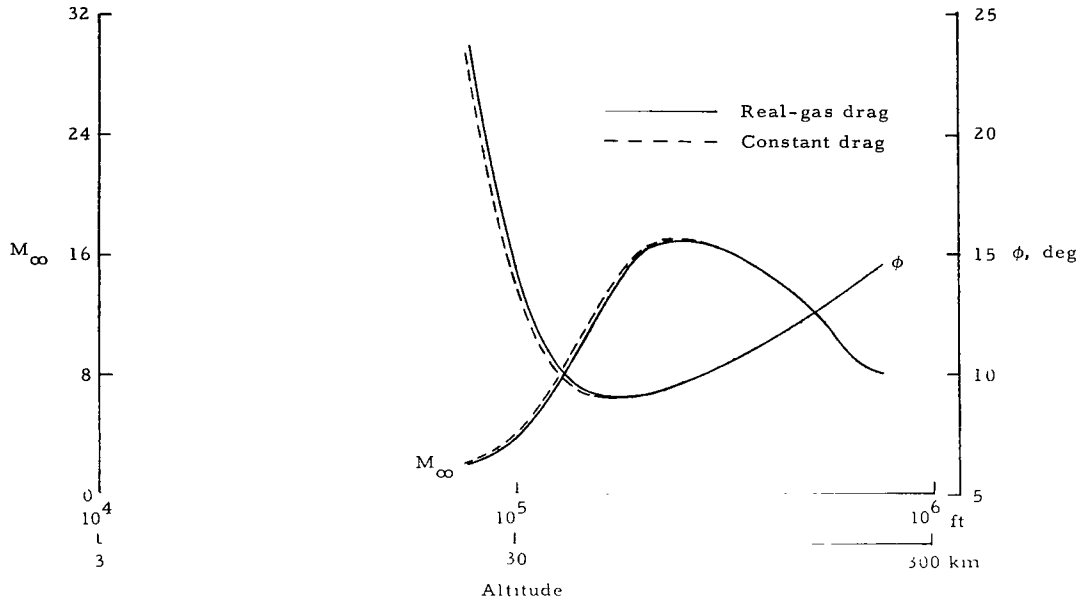

(e) Max H_ρ model atmosphere.

Figure 14.- Concluded.

TABLE III.- REAL-GAS AND CONSTANT-DRAG COEFFICIENT DETERMINATIONS OF V_∞, ϕ, AND H AT MACH 2.0

[V_E = 4.57 km/sec (15 000 ft/sec); $\phi_E = 15^\circ$]

Model atmosphere	Constant drag V_∞		Real-gas drag V_∞		Constant drag ϕ, deg	Real-gas drag ϕ, deg	Constant drag H		Real-gas drag H		Real-gas drag H minus constant drag H	
	m/sec	ft/sec	m/sec	ft/sec			m	ft	m	ft	m	ft
Max ρ_s	399.0	1309	398.4	1307	21.79	22.15	14 910	48 910	15 090	49 500	180	590
Mean	456.9	1499	456.3	1497	23.00	23.30	13 430	44 070	13 850	45 450	420	1380
Min ρ_s	489.8	1607	490.4	1609	23.81	24.01	10 700	35 090	11 340	37 210	650	2120
Min H_ρ	391.1	1283	389.5	1278	21.94	22.25	7 379	24 210	7 654	25 110	270	900
Max H_ρ	506.9	1663	506.3	1661	23.26	23.58	22 900	75 130	23 370	76 680	470	1550

therein that there are significant differences in altitudes but very small differences in flight-path angles and velocities. The altitude differences range from 180 meters (590 ft) for the Max ρ_s atmosphere to 650 meters (2120 ft) for the Min ρ_s atmosphere. For the Min H_ρ atmosphere, where a Mach number of 2 is reached at the lowest altitude, real-gas effects provided a 270-meter (900-ft) increase in altitude.

In connection with the Max H_ρ trajectory in figure 14(e) it should be noted that a substantial effort (see appendix C) was expended on the real-gas calculations above 90 km (295 000 ft). Subsequent simplified calculations using a constant C_D of 1.78 above 90 km (295 000 ft) and the real-gas C_D at lower altitudes yielded a trajectory which was in excellent agreement with the real-gas Max H_ρ model trajectory. It appears that the application of this simplified approach in determining trajectories for model atmospheres similar to the Max H_ρ atmosphere would be justified.

CONCLUDING REMARKS

The real-gas drag coefficient was found to vary from about 1.62 to 1.78 and to have a value near 1.75 at a maximum dynamic pressure for orbital entry into the five model Mars atmospheres considered:

Max H_ρ atmosphere	atmosphere with maximum average density scale height
Max ρ_s atmosphere	atmosphere with maximum density near surface
Mean atmosphere	mean model atmosphere
Min H_ρ atmosphere	atmosphere with minimum average density scale height
Min ρ_s atmosphere	atmosphere with minimum density near surface

For a given model atmosphere, very small differences in the drag coefficient occurred when entry conditions were varied over the ranges considered. However, the difference between the Mach number variation of drag coefficients for the Min ρ_s and Max ρ_s model atmospheres is about 3 percent and the other three generally fall between these two. The real-gas variation of drag coefficient with Mach number for the Max H_ρ model atmosphere was different in character from the variations of the other four model atmospheres.

The differences between real-gas drag coefficient trajectories and those obtained by using a constant drag coefficient of 1.61 were shown. At a Mach number of 2, there

were very small differences in flight-path angles and velocities but significant differences in altitudes, the Min ρ_s model atmosphere giving the largest difference (650 meters or 2120 ft). A Mach number of 2 is reached at the lowest altitude for the Min H_ρ model atmosphere, where real-gas effects provide a 270-meter (900-ft) increase in altitude.

Langley Research Center,
National Aeronautics and Space Administration,
Hampton, Va., January 21, 1971.

APPENDIX A

EQUATIONS OF MOTION

For completeness, the standard point mass trajectory equations for a nonlifting body are given in this appendix. The derivatives of the velocity, flight-path angle, and altitude are

$$\frac{dV_\infty}{dt} = g \sin \phi - \frac{\frac{1}{2}\rho_\infty V_\infty^2}{M/C_D A} \tag{A1}$$

$$\frac{d\phi}{dt} = -\frac{1}{V_\infty}\left(\frac{V_\infty^2}{r_S + H} - g\right)\cos \phi \tag{A2}$$

$$\frac{dH}{dt} = -V_\infty \sin \phi \tag{A3}$$

where

$$g = g_S\left(\frac{r_S}{r_S + H}\right)^2 \tag{A4}$$

APPENDIX B

SHOCK DENSITY RATIO DETERMINATION

The purpose of this appendix is to show how the shock density ratio ρ_S/ρ_∞ was computed from the instantaneous velocity and ambient conditions in the free-stream and equilibrium enthalpy as a function of pressure and density behind the shock. The oblique-shock equations (ref. 5) are solved by a procedure similar to that of reference 10.

The component of the free-stream velocity normal to the shock wave is

$$u_\infty = V_\infty \sin \theta \tag{B1}$$

where θ is a prescribed shock inclination angle. An initial estimate is made for the density behind the shock ρ_S and is used to compute the normal component of the velocity behind the shock:

$$u_S = \frac{\rho_\infty u_\infty}{\rho_S} \tag{B2}$$

The pressure and enthalpy behind the shock based on the estimated value for ρ_S are computed by using equations (B1) and (B2) and the ambient conditions:

$$p_S = -\rho_S u_S^2 + p_\infty + \rho_\infty u_\infty^2 \tag{B3}$$

$$h_S = -\frac{1}{2} u_S^2 + \frac{1}{2} u_\infty^2 + h_\infty \tag{B4}$$

Equilibrium enthalpy behind the shock is evaluated from polynomial curve fits of its variations with pressure p_S and density ρ_S. Since ρ_S is an estimated quantity, the enthalpy thus obtained agrees only approximately with that given by equation (B4). Additional values of density are substituted into the thermodynamic curve fit equations until the value of h_S obtained agrees with equation (B4) to within 100 m^2/sec^2 (1076 ft^2/sec^2). The value of density which provides the aforementioned enthalpy agreement is then substituted back into equation (B2) and the process is repeated. When two successive values of ρ_S (that is, those required to obtain enthalpy agreement) agree to within 10^{-3} percent, the calculation is terminated.

APPENDIX C

HIGH-ALTITUDE THERMODYNAMIC PROPERTIES FOR MAXIMUM H_ρ ATMOSPHERE

The interpolation routine which computes the equilibrium properties $h_S/R_U T_S$ and T_S at altitudes from 90 to 240 kilometers (295 000 to 787 000 ft) for the Max H_ρ model atmosphere is described in this appendix. Three sets of curve fits (polynomial

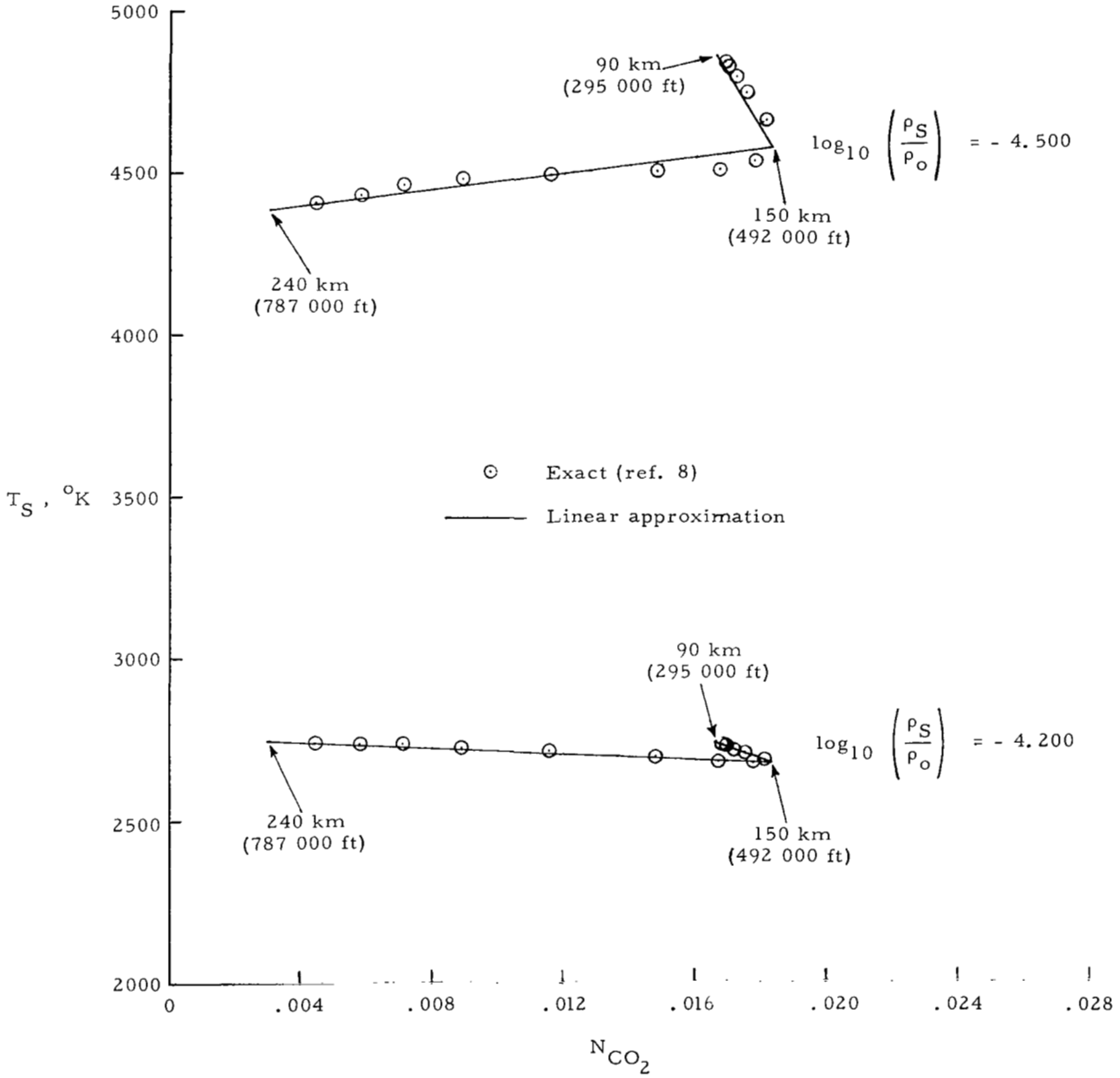

Figure 15.- Variation of temperature with the interpolation parameter N_{CO_2} for two densities at $p_S/p_o = 10^{-3}$ for the Max H_ρ atmosphere.

approximations of thermodynamic properties) are used, valid for the atmospheric compositions at 90, 150, and 240 kilometers (295 000, 492 000, and 787 000 ft). For a given pressure ratio and density ratio, each property is determined by linear interpolation from two of the three sets of thermodynamic-property curve fits. The interpolation parameter for h_S/R_UT_S is the molecular weight M_U of the undissociated gas mixture, that is, the mixture which would exist at low temperatures where all the CO and O are combined into CO_2 and O_2. The interpolation parameter for T_S is N_{CO_2} which is the number of moles of the element carbon per unit mass of the atmosphere (equal to the number of moles of CO_2 per unit mass of the undissociated mixture). These parameters were computed from the composition of the Max H_ρ model atmosphere (table II) and tabulated at 10-kilometer (32 800-ft) intervals for altitudes of 90 kilometers (295 000 ft) and higher.

Figures 15 and 16 show how well the linear interpolation procedure works for a pressure ratio of $p_S/p_o = 10^{-3}$ and two values of density ratio, $\rho_S/\rho_o = 10^{-4.2}$ and $10^{-4.5}$. The circled points are the exact values (ref. 8) whereas the straight-line segments represent the interpolation values. Circles were not placed around the points at altitudes of 90, 150, and 240 kilometers (295 000, 492 000, and 787 000 ft), since the straight lines were drawn by connecting these points. The differences between the exact values (circles) and the interpolated values (straight lines) are usually less than 2 percent.

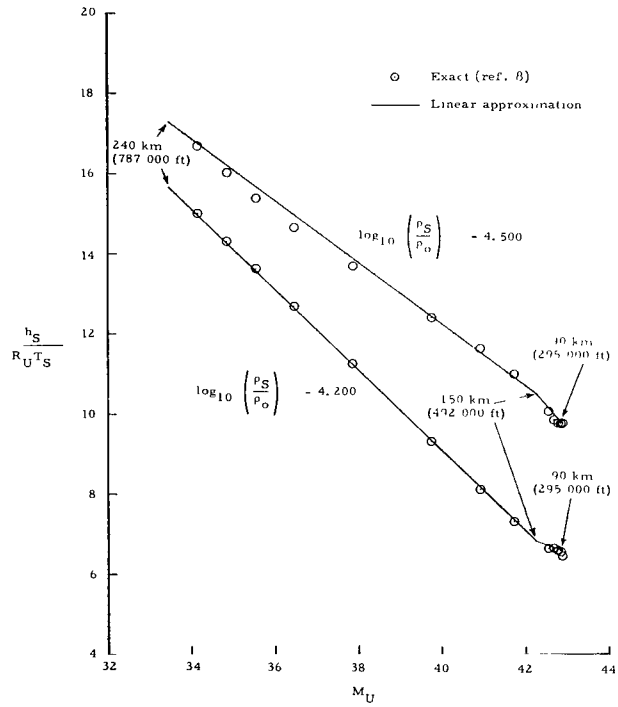

Figure 16.- Variation of the thermodynamic quantity h_S/R_UT_S with the interpolation parameter M_U for two densities at $p_S/p_o = 10^{-3}$ for the Max H_ρ atmosphere.

REFERENCES

1. Pragluski, William J.: Flight Mechanics of Unmanned Landers. AIAA/AAS Stepping Stones to Mars Meeting, Mar. 1966, pp. 107-115.

2. Pritchard, E. Brian; and Harrison, Edwin F.: Analysis of Mars Entry With Consideration of Separation and Line-of-Sight Relay Communication for Bus-Capsule Combinations. NASA TN D-2841, 1965.

3. Campbell, James F.: Supersonic Aerodynamic Characteristics and Shock Standoff Distances for Large-Angle Cones With and Without Cylindrical Afterbodies. NASA TN D-5334, 1969.

4. Walker, Billy; and Weaver, Robert W.: Static Aerodynamic Characteristics of Blunted Cones in the Mach-Number Range From 2.2 to 9.5. Tech. Rep. 32-1213 (Contract No. NAS 7-100), Jet Propulsion Lab., California Inst. Technol., Dec. 1, 1967.

5. Ames Research Staff: Equations, Tables, and Charts for Compressible Flow. NACA Rep. 1135, 1953. (Supersedes NACA TN 1428.)

6. South, Jerry C., Jr.: Calculation of Axisymmetric Supersonic Flow Past Blunt Bodies With Sonic Corners, Including a Program Description and Listing. NASA TN D-4563, 1968.

7. Krumins, Maigonis V.: Drag and Stability of Various Mars Entry Configurations. IAF Paper RE 138, Oct. 1968.

8. Allison, Dennis O.: Calculation of Thermodynamic Properties of Arbitrary Gas Mixtures With Modified Vibrational-Rotational Corrections. NASA TN D-3538, 1966.

9. Newman, Perry A.; and Allison, Dennis O.: Direct Calculation of Specific Heats and Related Thermodynamic Properites of Arbitrary Gas Mixtures With Tabulated Results. NASA TN D-3540, 1966.

10. Callis, Linwood B.; and Kemper, Jane T.: A Program for Equilibrium Normal Shock and Stagnation Point Solutions for Arbitrary Gas Mixtures. NASA TN D-3215, 1966.

NASA-Langley, 1971 —— 30 L-7522

02U 001 55 51 3DS 71043 00903
AIR FORCE WEAPONS LABORATORY /WLOL/
KIRTLAND AFB, NEW MEXICO 87117

ATT E. LOU BOWMAN, CHIEF, TECH. LIBRARY

"The aeronautical and space activities of the United States shall be conducted so as to contribute . . . to the expansion of human knowledge of phenomena in the atmosphere and space. The Administration shall provide for the widest practicable and appropriate dissemination of information concerning its activities and the results thereof."

— NATIONAL AERONAUTICS AND SPACE ACT OF 1958

NASA SCIENTIFIC AND TECHNICAL PUBLICATIONS

TECHNICAL REPORTS: Scientific and technical information considered important, complete, and a lasting contribution to existing knowledge.

TECHNICAL NOTES: Information less broad in scope but nevertheless of importance as a contribution to existing knowledge.

TECHNICAL MEMORANDUMS: Information receiving limited distribution because of preliminary data, security classification, or other reasons.

CONTRACTOR REPORTS: Scientific and technical information generated under a NASA contract or grant and considered an important contribution to existing knowledge.

TECHNICAL TRANSLATIONS: Information published in a foreign language considered to merit NASA distribution in English.

SPECIAL PUBLICATIONS: Information derived from or of value to NASA activities. Publications include conference proceedings, monographs, data compilations, handbooks, sourcebooks, and special bibliographies.

TECHNOLOGY UTILIZATION PUBLICATIONS: Information on technology used by NASA that may be of particular interest in commercial and other non-aerospace applications. Publications include Tech Briefs, Technology Utilization Reports and Technology Surveys.

Details on the availability of these publications may be obtained from:

SCIENTIFIC AND TECHNICAL INFORMATION OFFICE

NATIONAL AERONAUTICS AND SPACE ADMINISTRATION

Washington, D.C. 20546